RSC Advances

PAPER

View Article Online
View Journal | View Issue

Cite this: *RSC Adv.*, 2023, **13**, 9530

Ionic modification of graphene nanosheets to improve anti-corrosive properties of organosilicon composite coatings†

Kai Yao,[a] Hongxia Zhu,*[a] Yulu Wang,[a] Rong Luo,[a] Liqiang Jin,*[a] Lefu Xie[b] and Zhigang Tian[b]

Composite coatings with anti-corrosive properties were fabricated using quaternized silicone oil modified graphene oxide and silicone polymer. Quaternized silicone oil was successfully synthesized through copolymerization of octamethyl cyclotetrasiloxane (D4), chloropropylsilane and triethylamine. The quaternized silicone oil modified graphene oxide (M-GO) was characterized by using ^{1}H NMR, FT-IR, Small-angle X-ray scattering (SAXS), Thermogravimetry (TG) and Transmission electron microscopy (TEM). The results showed that the M-GO was formed successfully. The M-GO could be dispersed without aggregation in some organic solvents, and the concentration of M-GO could be up to 3 mg ml^{-1}. The M-GO-reinforced silicone composites exhibited obvious improvements in thermal stability, mechanical properties and especially anticorrosive properties with the highest E_{corr} (−121 mV) and the lowest I_{corr} (6.058 × 10^{-9} A cm^{-2}), and the protection efficiency of the matrix could reach 99.97%. The anticorrosive mechanism of the fabricated composite coatings was investigated. This work provides a ready strategy for modification of GO and fabrication of high performance graphene-based silicone composite materials.

Received 12th February 2023
Accepted 13th March 2023

DOI: 10.1039/d3ra00951c

rsc.li/rsc-advances

Introduction

Corrosion is an inevitable process in the world, and the annual economic loss caused by metal corrosion is an unignorable number.[1–3] Various surface protections have been developed to reduce the corrosion rate of metals, including chemical conversion, anodic oxidation, organic coatings and so on.[4] In recent years, the development of active organic anticorrosive coatings is considered to be one of the most promising methods in anti-corrosive applications.[5] Among these technologies, graphene-based polymer composite coatings have been paid more and more attention, because of their environmental friendliness, excellent chemical resistance, and high protection.[6] The main research types include the incorporation of graphene oxide and its derivatives into polymer-based structures.[7] However, GO is not conducive to anti-corrosion applications due to its hydrophilic tendency.[8] With the purpose of improving graphene's application performance, it is essential to disperse GO well to retain certain desirable physicochemical properties, such as high dispersibility, hydrophobicity and consistent interfacial activity in various organic and polymer matrixes.[9,10] The lamellar structure of graphene with huge π–π stacking will be prone to agglomerate in organic solvents and polymer matrixes. The distinctive 2D structure of graphene can be modified by functional molecules in order to improve its dispersibility in a polymer matrix.[11,12] Haddadi *et al.* used tannic acid (TA) as a reducing agent to reduce graphene oxide and combined with ceric cations (Ce^{3+}) to prepare nanoplatforms. The nanoplatforms have good dispersion in epoxy matrix, and the prepared coating has excellent mechanical strength and barrier ability, and has excellent long-term corrosion prevention effect.[13] Li *et al.* functionalized GO with tetraethoxysilane and prepared organofunctional silane composite coatings. It was found that the dispersibility of graphene was greatly improved.[14] Liang *et al.* modified GO using bis(triethoxysilylpropyl)tetrasulfide by electrophoretic deposition to prepare trilaminar structure coatings on the surface of Fe–W alloy. The composite coatings can effectively prevent the erosion of the substrate by water and corrosive molecules.[15] Many researches show that the dispersibility of graphene nanosheets in organic solvents can be improved significantly by chemical modifications.[16–19] Moreover, the modified nanosheets as an additive to the composite coatings can greatly improve the mechanical properties and corrosion resistance of the coating.[20–22]

Organosilicon materials are widely employed as coatings due to their stable thermal stability, excellent corrosive resistance,

[a]*State Key Laboratory of Biobased Material and Green Papermaking, Qilu University of Technology (Shandong Academy of Sciences), Jinan, 250353, Shandong, P. R. China. E-mail: hxzhu@qlu.edu.cn*

[b]*New Era Chemical Shandong Limited Liability Company, Weihai, 264200, Shandong, P. R. China*

† Electronic supplementary information (ESI) available. See DOI: https://doi.org/10.1039/d3ra00951c

environmental friendliness and desirable hydrophobic property.[23,24] Especially, the hybrid organosilicon materials formed by Si–O–Si bonds can effectively prevent the intrusion of corrosive agents.[25–27] The organosilicon composite coating with superior anticorrosive performance can be achieved by homogenous introduction of graphene nanosheets into organosilicon polymer matrix.[28] Therefore, it is necessary to form the organosilicon composite coating to improve its anticorrosion performance.

In this study, M-GO is designed and prepared by using the quaternized silicone prepolymer as the "bridge" to incorporate graphene nanosheets into silicone matrix. Then, graphene-based composite coatings with desired interfacial compatibility between graphene and organosilicon were prepared. The influence of modification on the thermal stability, dispersibility, and lattice structure of nanosheets has been investigated comprehensively. We also examined the effect of incorporating M-GO into the silicone on the composites' thermal and mechanical properties.

Results and discussion

Structure characterization of quaternized silicone oil

The chemical structure of the synthesized quaternized silicone oil was confirmed by ^{1}H NMR, and its spectrum was shown in Fig. S1.† The ^{1}H NMR spectrum showed a peak at $\delta = 3.48$ ppm that was characteristic of the proton of $SiCH_2CH_2CH_2Cl$ in the curve of Cl-silicone oil. After reaction with sodium iodide, the signal at $\delta = 3.18$ ppm was characteristic of the proton of $SiCH_2CH_2CH_2I$ in the curve of I-silicone oil. Furthermore, the peak at 3.73 ppm were attributed to the $SiCH_2CH_2CH_2N$ in the curve of quaternized silicone oil. This shifting signal of protons indicated the quaternized silicone oil was successfully synthesized by formation of chemical bond. As can be seen from the FT-IR diagram (Fig. S2†), the stretching vibration peaks at 1094.4 cm^{-1} and 1020.6 cm^{-1} were due to Si–O–C and Si–O–Si, respectively, and the stretching vibration peak at 802.7 cm^{-1} was from Si–C. For quaternized silicone oil, there is a new bending vibration peak of N–H at 1526.2 cm^{-1}. The GPC result indicated the M_w of quaternized silicone oil is 8341 g mol^{-1}. Combining the above-mentioned results, the quaternized silicone oil was successfully synthesized by formation of chemical bond.

Characterizations of GO and M-GO

FT-IR spectra of GO and M-GO composites are presented in Fig. 1a. The wide and strong stretching vibration peak at 3442.9 cm^{-1} belongs to –OH on the GO surface, while the peaks at 2314.6 cm^{-1} and 1652.1 cm^{-1} belong to C=O and the stretching vibration generated by –C=C, respectively. The

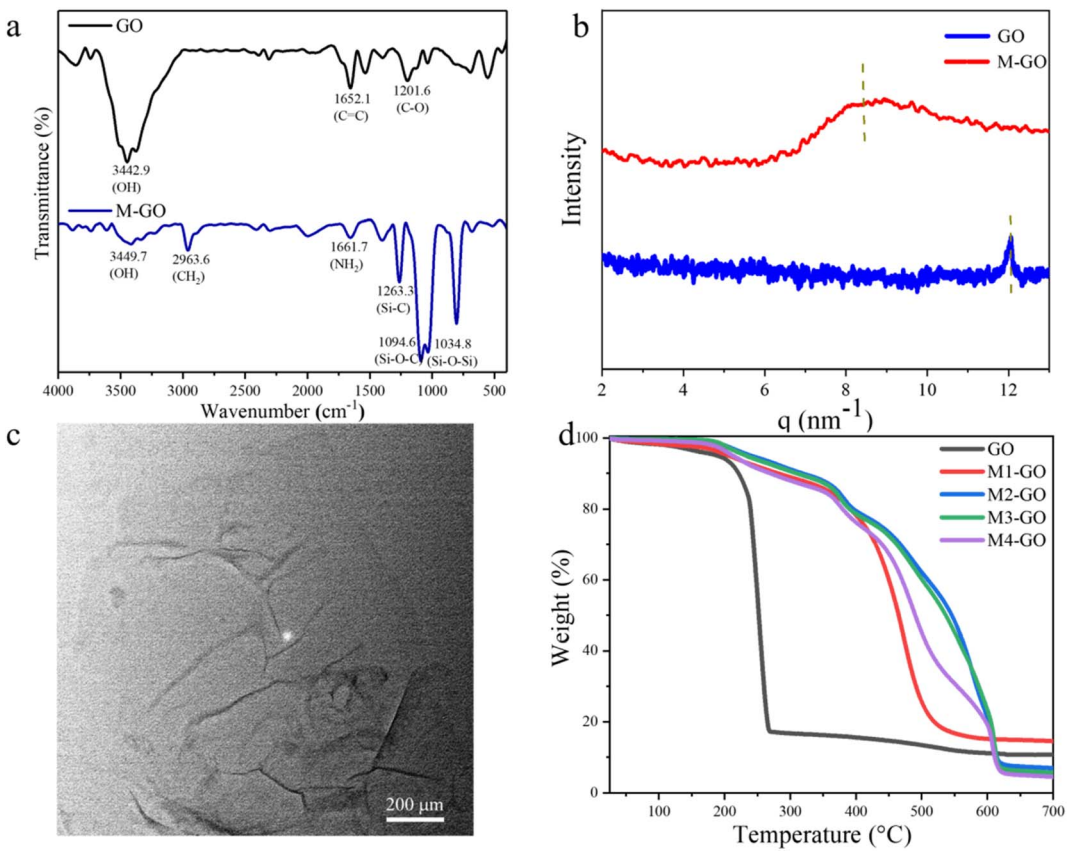

Fig. 1 (a) FTIR spectra of GO and M-GO; (b) Small angle X-ray scattering (SAXS) of GO and M-GO; (c)TEM image of dispersed M-GO in chloroform; (d) TGA curves for GO and M-GO.

Fig. 2 Solubility comparison diagram of GO and M-GO in different solvents.

transmittance peaks at 1201.6 cm^{-1} and 1040.6 cm^{-1} correspond to the bending vibration of C–O in benzene ring and epoxy group, respectively. In the case of M-GO, besides the same peaks as GO, 2963.6 cm^{-1} is the stretching vibration peak of CH_2, 1661.7 cm^{-1} is the bending vibration peak of NH_2, and 1263.3 cm^{-1}, 1094.6 cm^{-1}, 1034.8 cm^{-1} and 804.3 cm^{-1} correspond to Si–C, Si–O–C, Si–O–Si and Si–CH_3 bonds respectively. The results confirmed that the modification of GO by quaternized silicone oil is successful.[29,30] The Small-angle X-ray scattering results of GO and M-GO are shown in Fig. 1b. It can be clearly seen the spacing of graphene layers was enlarged by incorporation of silicone oil. The spatial configuration of graphene lamellar was also changed.[31] For GO, the scattering factor corresponding to the diffraction peak is $q = 12.05$ nm^{-1}, and the corresponding layer spacing is 0.73 nm. For M-GO, the scattering factor of modified graphene decreases to 8.44 nm^{-1} due to the silicone oils, and the layer spacing increases to 1.05 nm. In addition to increasing the distance between graphene nanosheets, it is obvious that small angle X-ray scattering peak presents a relatively broader peak, indicating that the whole material presents a disorder state inside. The regularity of graphene lamellar is significantly reduced, which is related to the introduction of quaternized silicone oil into the graphene lamellar structure. Different from the aggregation of graphene in organic solvents, the modified graphene can be well dispersed into organic solvents. The solubility comparison between GO and M-GO in different solvents has shown in Fig. 2 and can be summarized in Table 1. As we can see, GO can be stably dispersed in water, but can hardly be dispersed in chloroform, ethanol and other organic solvents. After modification, the layer spacing between graphene sheets increases, and π–π stacking force was reduced, and consequently the dispersibility of graphene sheets in organic solvents was enhanced. It can be dispersed well in chloroform and tetrahydrofuran, which will broaden its applied field. The TEM images show the modified graphene distribute uniformly in chloroform without aggregations (Fig. 1c). The large scale modified graphene can be obtained to a single layer structure with a few of wrinkle. The lamella structure of graphene is not destroyed in the modifying process. Meanwhile, the GO thin sheet structure was observed in organic solvent, providing more evidence for the successful chemical modification. The silicone modification enhanced the dispersion performance of graphene nanosheets. Thus, the modified graphene hybrid was available to act as nanofiller in polymer matrix to enhance the anti-corrosion performance of composites coating. In the Raman spectra (Fig. S3†), the G band and D band is located at 1597 cm^{-1} and 1329 cm^{-1}, which belong to the C=C of sp^2 hybridization in the graphene.[32] This result indicated the 2D structure of graphene was still remained without been destroyed by the modifying process. The UV spectrum of M-GO dissolved in chloroform is shown in Fig. S4.† It can be seen from the spectrum that in the measured range the intensity of characteristic absorption peak gradually increased with the increasing of concentration, and gradually red-shifted from 225 nm to 232 nm. The concentration of modified graphene can be up to 3 mg ml^{-1} in chloroform without aggregation. Compared with aggregation of graphene in organic solvent, the dispersibility of the modified graphene was greatly enhanced. The enhanced solubility of M-GO could be attributed to ionic silicone organic moieties, which decrease the layer-to-layer stacking so that organic solvent molecules can easily insert into the nanosheets through enlarged distances. The enhanced dispersibility of M-GO in organic solvents made it a favorable candidate for preparation of advanced silicone composite materials. Fig. 1d showed the thermogravimetric results of the GO and M-GO. Taking 10% weight loss temperature is the measurement standard for thermal stability.[33] The temperature of GO at 10% thermogravimetric weight loss is 221.51 °C, while the temperatures of M-GO are 287.86 °C, 327.56 °C, 312.02 °C and 271.85 °C, respectively, indicating that the thermal stability of M-GO composites was significantly improved after modification by quaternized silicone oil. Among the M-GO composites, M2-GO has the best thermal stability, which is 106.05 °C higher than GO at the 10% weight loss. The reason for the increment in thermal stability can be due to the strong crosslinking interaction between GO and silicone oil networks.

Characterizations of composites coatings

As we can see from Fig. 3, the composite coatings with GO as additive had a lot of aggregations, while the surface of PDMS coatings with M-GO as additives were smooth and flat. This result indicates that the dispersibility of GO in polysiloxane was poor while the dispersibility of M-GO was greatly improved.

Table 1 Solubility comparison of GO and M-GO in different solvents

Solvent	H_2O	Methanol	Ethanol	Acetone	$CHCl_3$	THF	DMSO	DMF
GO	++	−−	+−	−−	−−	−−	++	++
M-GO	++	+−	+−	+−	++	++	+−	++

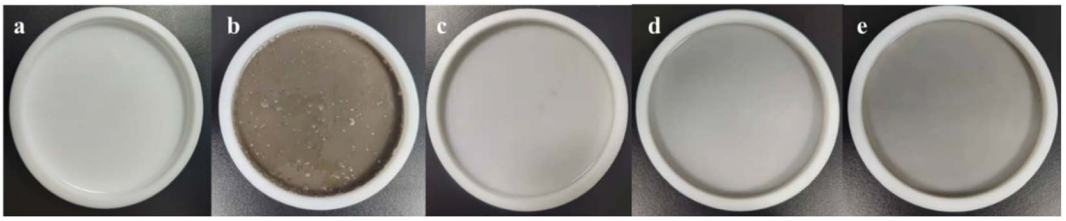

Fig. 3 Preparation of composites coatings (a: silicone coating; b: silicone coating with GO as additive; c, d, and e: silicone coatings with 5%, 10%, and 15% M-GO as additives, respectively).

The cross-sectional images of pure silicone polymer, silicone polymer with GO, silicone polymer with modified graphene coatings are shown in Fig. 4 and Fig. S5.† It could been seen that the cross-sectional surface of pure silicone coatings were relatively smooth, while the cross-sectional surface of silicone polymer with modified graphene coatings were rough, indicating the composite coatings with M-GO were more flexible. This result is in accordance with mechanical properties of Fig. 4f, we will further discuss it. In addition, it's clear that there are no obvious cracks and holes on the cross-sectional surface of silicone polymer with modified graphene, indicating that the structure is integrity and has a good resistance to the invasion of corrosive media. The top surface morphologies of cross-sectional coatings are shown in Fig. 4c and d. The color variation refers to the changes of coating surface roughness. It can been seen that the surface of pure silicone coating is smooth, and the surface roughness of composite coatings increased obviously after adding M-GO as additives. Moreover, surface roughness is related to the water contact angles,[34] and the surface will be more hydrophobic when the surface roughness increases for the hydrophobic surface.

The water contact angle (CA) of different coatings were shown in Fig. 4e. The CA of pure silicone coating is only 102.6°, which is favorable for water as well as corrosive medium to adhere and leads to corrosion on the metal surface. The CA of silicone polymer with modified graphene composite coatings increased with the increasing of M-GO's content and the maximum of CA can reach 143.7° when the M-GO content reaches 15%. Silicone composite coating MGO-SC3 has the best hydrophobicity, the incorporated of graphene nanosheets can great enhanced the surface can effectively prevent water and corrosion medium from penetrating through the coatings which is consistent with the conclusion of surface roughness above. The mechanical properties and folding resistance of the different coatings are shown in Fig. 4f. As can be seen, the elongation at break of pure silicone coating is 180.93%, and the tensile strength is 2.71 MPa. After the addition of GO, both the elongation at break strength of the composite coating decrease, may result from the GO aggregation which destroys the uniformity of coating and consequently deteriorate the mechanical property. In contrast, the mechanical properties of silicone composite coatings with modified graphene are

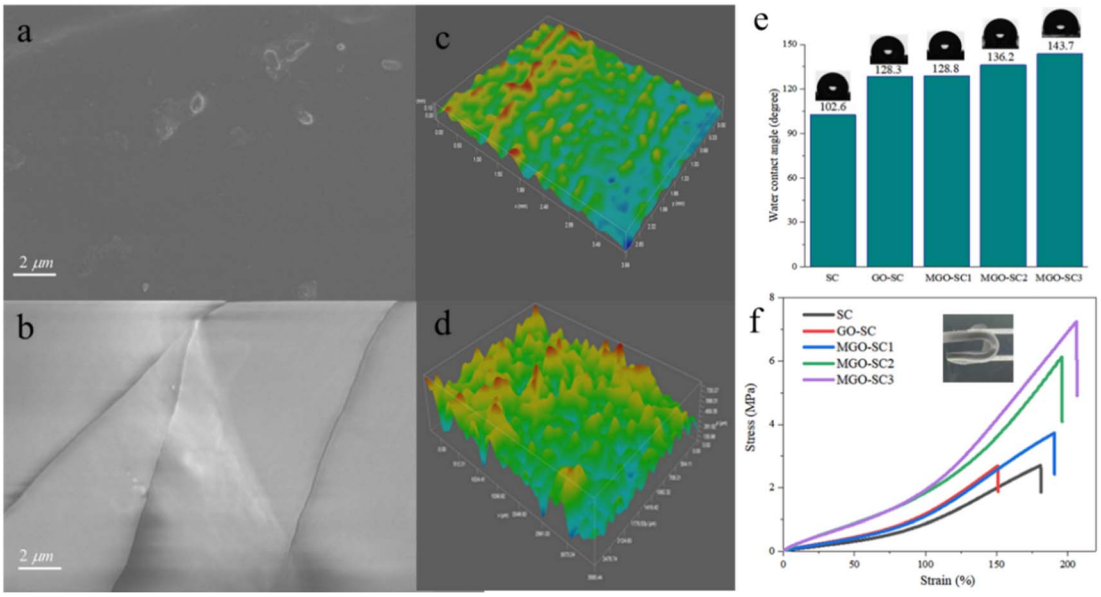

Fig. 4 SEM cross-sectional images of pure silicone coating (a) and silicone coating with M-GO (b); Surface morphologies of pure silicone coating (c) and silicone coating with 15% M-GO as additives (d) by AFM; (e) water contact angle of different coating surfaces. (f) Mechanical properties (inset is folding resistance of coating with 15% M-GO).

gradually improved with the increasing amount of M-GO. The elongation at break reached 208.96% (MGO-SC3), 15.49% higher than that of the pure silicone coating, and its tensile strength is up to 7.24 MPa, increased by 167.16%. The reason is that the dispersion of nanosheets in composites have been improved after modification. In addition, the crosslinking of silicone oil chain in M-GO enhances its mechanical properties. The prepared all coatings have excellent folding resistance and can be restored to their original appearance after bending.

Anticorrosive properties of composite coatings

The Tafel test results of different coatings are shown in Fig. 5a and corrosive results are presented in Table. S1,† in which E_{corr} refers to the corrosion potential and I_{corr} is corrosion current density. Usually, lower I_{corr} and higher E_{corr} mean lower corrosion rate and better overall anticorrosion properties of coatings.[35,36] Furthermore, b_a, b_c and PEF represent the anodic slope, cathodic slope, and coating protection efficiency, respectively. The protection efficiency (P_{EF}) is calculated through the eqn (1) below.

$$P_{EF}\ (\%) = (I_{corr}(\text{Bare}) - I_{corr}(\text{Coating})) / I_{corr}(\text{Bare}) \times 100\% \quad (1)$$

As can be seen from Fig. 5a, the E_{corr} and I_{corr} of bare copper are −287 mV and 1.807×10^{-5} A cm^{-2}, respectively. Compared with bare Cu substrate, the Tafel plots of the coated samples shifted to higher potential. When silicone coating is applied to Cu substrate, E_{corr} increases and I_{corr} decreases, and when 10% GO is added to silicone coating, the E_{corr} increases to −198 mV and I_{corr} decreases to 1.799×10^{-6} A cm^{-2}. When M-GO is used as additive, E_{corr} increases and I_{corr} decreases further with the increase of its additive amount. It can be concluded that the addition of M-GO compound significantly improves the corrosion resistance of composite coatings, and the corrosion resistance is best when the addition amount is 15% with the highest E_{corr} (−121 mV) and lowest I_{corr} (6.058×10^{-9} A cm^{-2}), which is 4 orders of magnitude lower than that of Cu matrix. Moreover, the protection efficiency of the coating can reach 99.97%.

EIS measurements are used to test the anti-corrosive performance of pure Cu, SC, GO-SC, MGO-SC composite coatings, and the results are shown in Fig. 5b. As we can see that radians are increasing significantly after the addition of M-GO. Generally speak, larger arc radius means better anticorrosion properties. It is obvious that the addition of GO and M-GO can effectively improve the electrochemical performance of silicone coatings. Compared with other coatings, MGO-SC3 silicone composite coating has the best protection performance. The corresponding values of their equivalent circuits are listed in Table S2.† R_{coat} is the coating resistance, CPE_{coat} is the coating capacitance, R_{it} is the interface transfer resistance, and CPE_{dl} is the double electric layer capacitance. The coating resistance (R_{coat}) increases gradually with the increase of M-GO content. R_{coat} of pure PDMS is 2.20×10^3 Ω cm^2, and R_{coat} of MGO-SC3 is 5.78×10^5 Ω cm^2. Chi squared (χ^2) is also given in Table S2,† which can indicate the accuracy of fitting results. The Bode plots of various composite coatings are shown in Fig. 5b and S9.† The Bode curve contains low frequency and high frequency regions, which are related to the capacitance and electron transport capacity of the coating, respectively. The low frequency area impedance modulus value (0.01 Hz) $|Z|$ is a quantitative indicator for coating protective ability. In low frequency range (0.01 Hz), samples of coating impedance values $|Z|$ obviously higher than that of bare copper impedance value (1.28 kohm cm^2), of which impedance value of MGO-SC3 is the highest, reaching (4.39 MΩ cm^2). The corrosion rate is inversely proportional to the impedance modulus in the low-frequency region, MGO-SC3 has the lowest corrosion rate, which is consistent with the conclusion obtained by Tafel curves and Nyquist plots. Therefore, M-GO can effectively prevent the invasion of corrosive media. Compared with GO composite coatings, the corrosion resistance of composites coating with M-GO was greatly improved due to the desired dispersion of nanosheets.

Fig. 6 represents the anticorrosive mechanism of silicone composite coatings. In general, the corrosion process of the

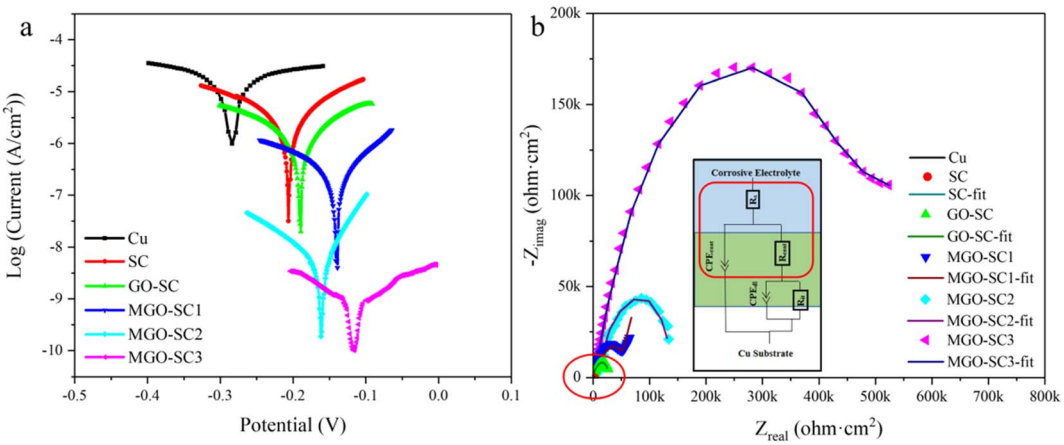

Fig. 5 (a) Tafel curves of different coatings in 3.5 wt% NaCl solution. (b) Nyquist plots of Cu and PDMS, PDMS/GO and PDMS/M-GO composite coatings (Embedded graph is equivalent circuit of MGO-SC, and in the red frame is in accordance with SC and GO-SC.).

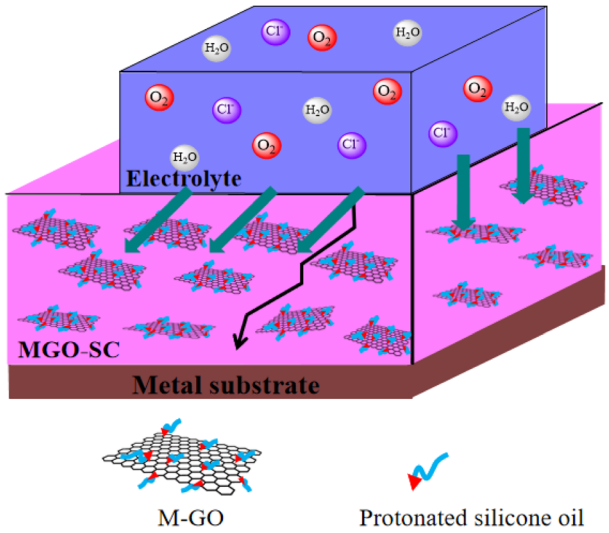

Fig. 6 Anti-corrosive mechanism of silicone composite coating.

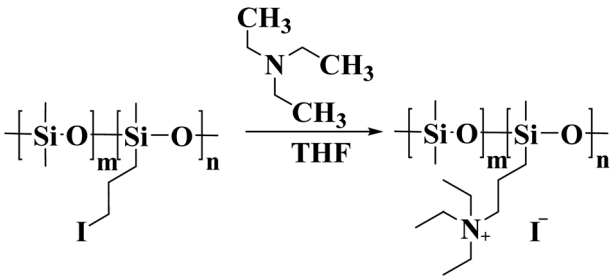

Fig. 7 The synthesis of quaternized silicone oil.

coated metal matrix generally includes absorption of corrosive agents on coating, diffusion of corrosive ions within the coating, and arrival of corrosive ions at the coating/metal interface.[37] The addition of graphene nanosheets to silicone coating significantly enhances the barrier properties of coating and reduces the defects and micropores of coating. The good dispersion of M-GO gives a dense and uniform barrier which can prevent the diffusion of water, chloride ion, oxygen from coating to substrate. On one hand, the introduction of M-GO exhibit a barrier effect and prolong the diffusion pathway of the corrosion ions. Therefore, lower amount of corrosion products, rusts, and blisters are formed. On the other hand, the cross linking between the coating and the matrix can be enhanced due to the formation of Si–O–Si network structure after GO modification. Based on the synergistic effect mentioned above, the composite coating exhibits good anti-corrosion performance.

Experimental

Materials and methods

Graphene oxide (GO) was supported from Zhejiang Gaoxi Tech Co., Ltd.; dichloromethane (AR) and chloroform (AR) were purchased from Tianjin Fuyu Chemical Co., Ltd. Sodium iodide (NaI) was purchased from Shanghai Macklin Bio Co., Ltd. Triethylamine and tetrahydrofuran (THF) were purchased from Shanghai Hushi Chemical Co., Ltd. Deionized (DI) water was purified by using a UPH-IV ultrapure water apparatus (China) with a resistivity of 18.25 MΩ cm. Copper (Cu) sample is round with a radius of 0.50 cm and a thickness of 0.20 cm.

Synthesis of quaternized silicone oil

Iodopropyl silicone (for synthesized details, see the experimental section in the ESI Fig. S10 and S11†) was dissolved in tetrahydrofuran solvent, and the excess triethylamine (3.42 g, 0.0336 mol) was dropped. The mixture was stirred at 40 °C for 72 hours. Then, the tetrahydrofuran solvent was removed by rotary evaporation, and the unreacted triethylamine was removed by repeated washing with ethanol. The schematic diagram of synthesis process is shown in Fig. 7. ^{1}H NMR of quaternized silicone oil (400 MHz, $CDCl_3$, 298 K): a: 3.62 (t, 2H, Cl–CH_2–); b: 3.27 (t, 2H, I–CH_2–); c: 3.07 (t, 2H, $N(CH_2CH_3)_3$–CH_2–); d: 1.76 (d, 2H, –CH_2–); e: 0.61 (m,–2H, Si–CH_2–); f: 1.30 (d, 3H, –NCH_2CH_3).

The preparation process of M-GO

The preparation process of M-GO is shown in Fig. 8. The graphene was pre-treated with 0.1 mol L^{-1} sodium hydroxide solution, firstly. The pre-treated graphene and quaternized silicone oil were dissolved in water and chloroform under stirring with the concentration of 1 mg ml^{-1} and 10 mg ml^{-1}, respectively. Both solutions were mixed at a volume ratio of 1 : 1 in a glass bottle, forming a clear phase boundary with the dark aqueous solution of graphene oxide at the top and the yellowish chloroform solution of iodopropyl silicone oil at the bottom. After being stirred for 1 hour, phase transfer occurred with the migration of the dark graphene oxide from the top phase to the bottom (Fig. 9). The black modified graphene was obtained after the evaporation of the volatile compounds.

Preparation of silicone composite coatings with different content of M-GO (MGO-SC)

The M-GO composite coatings with different contents (5, 10, 15 wt%) of M-GO as additive were prepared. We called the different contents 5, 10, 15 wt% of M-GO silicone composites were MGO-SC1, MGO-SC2, MGO-SC3, respectively. The M-GO, poly(-dimethyl-methylvinylsiloxane) (Vi-PDMS) and poly(dimethyl-methylhydrogensiloxane) (H-PDMS) were mixed into a 250 ml three-necked flask, then sonicating for 15 min and stirring for 1 hour. The mass ratio of Vi-PDMS and H-PDMS is 10 : 1. After well dispersity, the platinum catalyst is dropped into and stirred clockwise for more than five minutes. After that, the coatings were prepared by pouring the mixture into Teflon moulds or by applying the mixture evenly on the surface of the pretreated copper sheet by the blade coating method, and then dried under vacuum at 60 °C for 24 hours to dry completely. The pure polysiloxane coating and the silicone composite coatings with graphene oxide (10 wt%) without modification as additives were used as the reference.

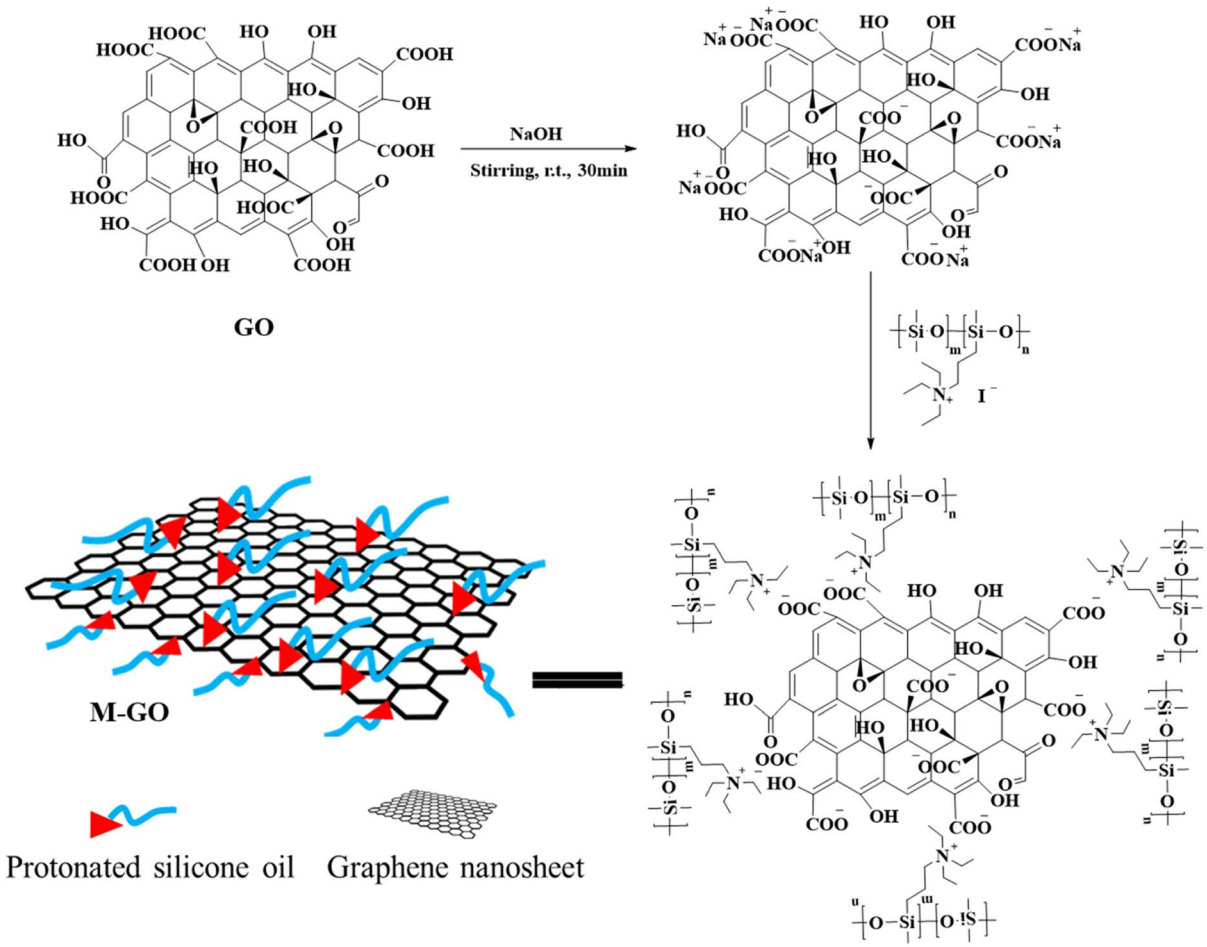

Fig. 8 Schematic diagram of GO modification process.

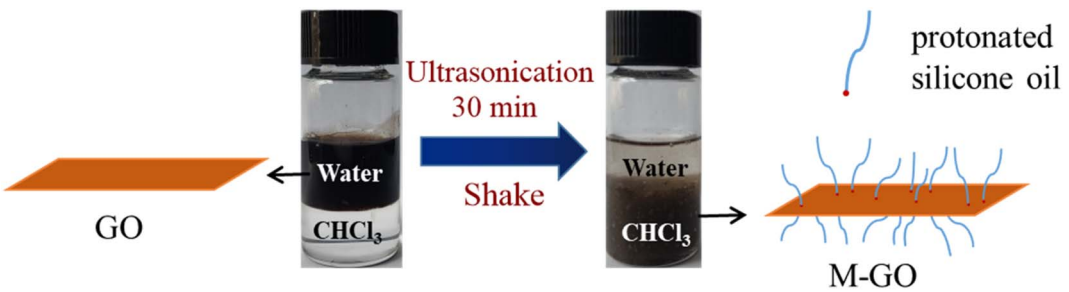

Fig. 9 Diagram of phase transfer process.

Conclusions

In summary, modified GO nanosheets with quaternized silicone oil are prepared *via* a ready and visual method. The distances of nanosheets were enlarged from 0.73 nm to 1.05 nm according to SAXS results. The M-GO also presents greatly enhanced thermal stability as well as good dispersibility in both water and organic solvents. The content of M-GO can be up to 3 mg ml^{-1} in chloroform. After polymerization with M-GO, the obtained graphene-reinforced silicone composites exhibit obvious improvements in thermal stability, mechanical property and hydrophobicity. The morphology, microstructure, and anticorrosive mechanism of the developed composite coatings were investigated. The MGO-SC3 has the best corrosion resistance with the largest E_{corr} and the smallest I_{corr}, and the protection efficiency can reach 99.97%. The graphene-reinforced composites coatings show enhanced anticorrosion capability compared to pure silicone composites, demonstrating their great potential for applications in corrosion-resistant coating and packaging fields. This developed approach provides a new

path to fabricate high performance graphene-based polymer composite materials.

Conflicts of interest

There are no conflicts to declare.

Acknowledgements

The authors are grateful for the financial support of National Natural Science Foundation of China (No. 22078165 and 21978139); Shandong Provincial Natural Science Foundation (No. ZR2020QB112); Young Doctoral Innovation Funds (2022PX062) of Qilu University of Technology; Foundation (ZR20190104) of State Key Laboratory of Biobased Material and Green Papermaking, Qilu University of Technology, Shandong Academy of Sciences.

Notes and references

1 S. Böhm, Graphene against corrosion, *Nat. Nanotechnol.*, 2014, **9**, 741.
2 C. Zhang, W. Li, C. Liu, *et al.*, Effect of covalent organic framework modified graphene oxide on anticorrosion and self-healing properties of epoxy resin coatings, *J. Colloid Interface Sci.*, 2022, **608**, 1025–1039.
3 A. Das, K. Maji, S. Naskar, *et al.*, Facile optimization of hierarchical topography and chemistry on magnetically active graphene oxide nanosheets, *Chem. Sci.*, 2020, **11**, 6556–6566.
4 G. Cui, Z. Bi, S. Wang, *et al.*, A comprehensive review on smart anti-corrosive coatings, *Prog. Org. Coat.*, 2020, **148**, 105821.
5 N. Keshmiri, P. Najmi, M. Ramezanzadeh, *et al.*, Designing eco-friendly lanthanide-based metal organic frameworks (MOFs) assembled graphene-oxide with superior active anti-corrosion performance in epoxy composite, *J. Cleaner Prod.*, 2021, **319**, 128732.
6 S. Dmitry and M. Helmuth, A Coat of Many Functions, *Science*, 2013, **341**, 1458–1459.
7 N. Keshmiri, P. Najmi, B. Ramezanzadeh, *et al.*, Superior thermal-mechanical properties of the epoxy composite reinforced with rGO-ATMP; Combined DFT-D theoretical modeling/experimental studies, *J. Mol. Liq.*, 2021, **331**, 115800.
8 N. Keshmiri, P. Najmi, B. Ramezanzadeh, *et al.*, Nano-scale P, Zn-codoped reduced-graphene oxide incorporated epoxy composite; synthesis, electronic-level DFT-D modeling, and anti-corrosion properties, *Prog. Org. Coat.*, 2021, **159**, 106416.
9 L. Rui, Y. X. Xu, W. F. Pu, *et al.*, Oligomeric ethylene-glycol brush functionalized graphene oxide with exceptional interfacial properties for versatile applications, *Appl. Surf. Sci.*, 2022, **606**, 154856–154870.
10 K. Gupta, S. R. Yasa, A. Khan, *et al.*, Charge-driven interaction for adsorptive removal of organic dyes using ionic liquid-modified graphene oxide, *J. Colloid Interface Sci.*, 2022, **607**, 1973–1985.
11 J. Suzuki, A. Ishizone, J. Sato, *et al.*, Amorphous flexible covalent organic networks containing redox-active moieties: a noncrystalline approach to the assembly of functional molecules, *Chem. Sci.*, 2020, **11**, 7003–7008.
12 J. Cao, Y. Chen, X. Wang, *et al.*, Janus sulfonated graphene oxide nanosheets with excellent interfacial properties for enhanced oil recovery, *Chem. Eng. J.*, 2022, **443**, 136391.
13 S. A. Haddadi, P. Najmi, N. Keshmiri, *et al.*, Cerium-doped tannic acid-reduced graphene oxide nanoplatform/epoxy nanocomposite coatings with enhanced mechanical and Bi-functional corrosion protection properties, *Composites, Part B*, 2022, **239**, 109969.
14 J. Li, J. C. Cui and J. Y. Yang, Silanized graphene oxide reinforced organofunctional silane composite coatings for corrosion protection, *Prog. Org. Coat.*, 2016, **99**, 443–451.
15 J. F. Liang, X. W. Wu, Y. H. Ling, *et al.*, Trilaminar structure hydrophobic graphene oxide decorated organosilane composite coatings for corrosion protection, *Surf. Coat. Technol.*, 2018, **339**, 65–77.
16 Y. Wang, S. S. Li, H. Y. Yang, *et al.*, Progress in the functional modification of graphene/graphene oxide: A review, *RSC Adv.*, 2020, **10**, 15328–15345.
17 J. Liu, J. Tang and J. J. Gooding, Strategies for chemical modification of graphene and applications of chemically modified graphene, *J. Mater. Chem.*, 2012, **22**, 12435–12452.
18 R. Trusovas, G. Račiukaitis, G. Niaura, *et al.*, Recent advances in laser utilization in the chemical modification of graphene oxide and its applications, *Adv. Opt. Mater.*, 2016, **4**, 37–65.
19 C. Liu, X. Huang, Y. Y. Wu, *et al.*, Review on the research progress of cement-based and geopolymer materials modified by graphene and graphene oxide, *Nanotechnol. Rev.*, 2020, **9**, 155–169.
20 J. Nie, D. Liu, S. Li, *et al.*, Improved dispersion of the graphene and corrosion resistance of waterborne epoxy–graphene composites by minor cellulose nanowhiskers, *J. Appl. Polym. Sci.*, 2019, **136**, 47631.
21 Y. Li, N. Zhang, L. Liu, *et al.*, Preparation of Phosphorus-containing Graphene and Corrosion Resistance of Composite Coating, *Chin. J. Mater. Res.*, 2022, **36**, 933–944.
22 X. Liu, S. Chen, Y. Zhang, *et al.*, Preparation of graphene oxide–boron nitride hybrid to reinforce the corrosion protection coating, *Corros. Rev.*, 2021, **39**, 123–136.
23 U. Eduok, O. Faye and J. Szpunar, Recent developments and applications of protective silicone coatings: A review of PDMS functional materials, *Prog. Org. Coat.*, 2017, **111**, 124–163.
24 M. Y. Jiang, L. K. Wu, J. M. Hu, *et al.*, Silane-incorporated epoxy coatings on aluminum alloy (AA2024). Part 1: Improved corrosion performance, *Corros. Sci.*, 2015, **92**, 118–126.
25 C. M. Wang, J. Shen, X. K. Zhang, *et al.*, In vitro degradation and cytocompatibility of a silane/$Mg(OH)_2$ composite coating on AZ31 alloy by spin coating, *J. Alloys Compd.*, 2017, **714**, 186–193.
26 Y. S. H. Xu, M. H. Li and M. Y. Liu, Corrosion and fouling behaviors of phosphatized Q235 carbon steel coated with

fluorinated polysiloxane coating, *Prog. Org. Coat.*, 2019, **134**, 177–188.

27 X. L. Huang, R. Ke and Y. S. Dong, Characterization and corrosion protection of nano-titanium dioxide doped BTSE-GPTMS sol-gel coating on cast Al–Si alloy, *J. Sol-Gel Sci. Technol.*, 2020, **94**, 671–680.

28 H. X. Zhu, Y. Y. Chen, H. Y. Li, *et al.*, In Situ Polymerization Approach to Graphene-Oxide-Reinforced Silicone Composites for Superior Anticorrosive Coating, *Macromol. Rapid Commun.*, 2019, **40**, 1800252.

29 W. J. Li, X. Z. Tang, H. B. Zhang, *et al.*, Simultaneous surface functionalization and reduction of graphene oxide with octadecylamine for electrically conductive polystyrene composites, *Carbon*, 2011, **49**, 4724–4730.

30 M. B. Kale, Z. Luo, X. Zhang, *et al.*, Waterborne polyurethane/graphene oxide-silica nanocomposites with improved mechanical and thermal properties for leather coatings using screen printing, *Polymer*, 2019, **170**, 43–53.

31 A. H. Li, S. F. Chen, Z. D. Ma, *et al.*, Corrosion protection properties of polyvinyl butyral/polyaniline-graphene oxide/poly (methylhydrosiloxane) composite coating for AA2024 aluminum alloy, *Diamond Relat. Mater.*, 2021, **116**, 108397.

32 R. Zhou, H. Y. Jin, N. K. Gao, *et al.*, Effect of Surface Roughness on Superhydrophobicity of Silicone Rubber Materials, *China Surf. Eng.*, 2009, **22**, 30–35.

33 R. N. Wenzel, Resistance of solid surfaces to wetting by water, *Trans. Faraday Soc.*, 1936, **28**, 988–994.

34 Y. Zhao, J. Q. Ma, K. Chen, *et al.*, One-Pot Preparation of Graphene-Based Polyaniline Conductive Nanocomposites for Anticorrosion Coatings, *Nano*, 2017, **12**, 1750056.

35 M. A. Raza, R. Z. U. Rehman and F. A. Ghauri, Corrosion study of silane-functionalized graphene oxide coatings on copper, *Thin Solid Films*, 2018, **663**, 93–99.

36 A. Diraki and S. Omanovic, Smart PANI/epoxy anti-corrosive coating for protection of carbon steel in sea water, *Prog. Org. Coat.*, 2022, **168**, 106835.

37 N. H. Othman, *et al.*, Graphene-based polymer nanocomposites as barrier coatings for corrosion protection, *Prog. Org. Coat.*, 2019, **135**, 82–99.